Available online at www.sciencedirect.com
SCIENCE DIRECT®
Journal of Solid State Chemistry 178 (2005) 3352–3358
JOURNAL OF SOLID STATE CHEMISTRY
www.elsevier.com/locate/jssc

S-, N- and C-doped titanium dioxide nanoparticles: Synthesis, characterization and redox charge transfer study

K. Madhusudan Reddy, Babita Baruwati, M. Jayalakshmi, M. Mohan Rao, Sunkara V Manorama*

Inorganic and Physical Chemistry Division, Indian Institute of Chemical Technology, Hyderabad 500 007, India

Received 28 June 2005; received in revised form 19 August 2005; accepted 22 August 2005
Available online 30 September 2005

Abstract

Herein we report on the synthesis and characterization of TiO_2 nanomaterials doped with anions like sulfur, carbon and nitrogen. Upon doping, the absorption extends well into the visible region. This shift in the absorption edge is accompanied by a concomitant narrowing of band gap. The resulting anion-doped TiO_2 nanomaterials were characterized by XRD, XPS, elemental analysis, EDAX, TEM, UV-DRS, DC conductivity, AC impedance and cyclic voltammetric studies. XPS confirms the presence of the dopants and the elemental analysis determined the amount of dopants in TiO_2. Electrochemical characterization was carried out by cyclic voltammetry at pHs 2, 6.5 and 10. As against the response of undoped TiO_2, the doped samples show an active electrochemical response indicating an induced charge transfer across the titania/solution interface, thus forming two anodic peaks and a cathodic peak. This interesting and significant observation was understood in terms of band bending due to anion doping as well as to the pH changes in the experimental solutions.

Keywords: Anion doping; Electrochemical response; Band bending

1. Introduction

Photovoltaic solar cells or dye-sensitized solar cells (DSSCs) fulfill the dream of scientists and industrialists trying to capture the solar energy and turn it into valuable and strategically important electric energy. Identifying the factors limiting the performance of cost-effective and non-toxic semi-conducting materials for harvesting solar energy and finding new ways and means to improve their performance remains a challenge that has become a thrust area of research worldwide. Of the new materials being developed for photovoltaic, photocatalytic and other applications, titanium dioxide (TiO_2) remains one of the most promising material because of its high efficiency, low cost, chemical inertness, eco-friendly nature and photostability. Nevertheless, TiO_2 with a wide band gap of 3.2 eV becomes active only under ultraviolet (UV) light that forms about 5–8% of the solar spectrum and is the principal drawback for its effective utilization. Thus, to improve the photoactivity of TiO_2, it is mandatory to extend its absorption into the visible region of the spectrum. This opens up another field of application for TiO_2, viz. semiconductor photocatalysis that is one of the most efficient methodologies for the oxidation processes wherein solar energy is utilized to degrade organic pollutants in air and water. Usually anchoring low band gap organic dyes on to the surface of TiO_2 does this, and this is being implemented successfully in DSSCs. Nonetheless, the ruthenium dyes are expensive and unstable in aqueous solutions leaving open questions regarding the long-term stability of these dyes [1]. In search of other approaches, doping of transition metals into TiO_2 and synthesis of reduced TiO_x have been adopted, but the

*Corresponding author. Fax: +91 40 2716 0921.
E-mail address: manorama@iict.res.in (S.V. Manorama).

0022-4596/$ - see front matter © 2005 Elsevier Inc. All rights reserved.
doi:10.1016/j.jssc.2005.08.016

thermal instability and an increase in charge carrier recombination centers have limited the performance of these materials [2,3].

A recent innovative technique involves the doping of TiO_2 with anions resulting in a desired band gap narrowing and an enhancement in the photodegradation efficiency under visible light [4]. Doping anions, like N, S, and C alters the conductivity and optical properties as they introduce new surface states that may lie close to the conduction band or valence band of TiO_2. Recent reports have shown that TiO_2 doping with N, C, S, etc., showed high photocatalytic activity under visible light owing to band gap narrowing. These applications demand TiO_2 with specifications of a band gap in the visible range. Bisquert et al. [5] have studied the charge carrier characteristics and kinetics of nanocomposite TiO_2 for solar cells. A first time report on photoelectrochemical and optical properties of nitrogen-doped titanium dioxide thin films prepared by reactive DC magnetron sputtering showed an enhancement in photoinduced current around 200 times higher than that for pure TiO_2 electrodes and generation of dioxygen from water by illumination of $TiO_{2-x}N_x$ electrodes at moderate anodic potentials [6]. The plausible reason behind this interesting behavior was the introduction of new surface states close to the valence band of TiO_2 brought about by the doped N anions. Substitutional doping of nitrogen was found to be effective because its *p* states contribute to the band gap narrowing by mixing with O2*p* states. In photoelectrochemical measurements, charge–hole recombination to a large extent pose hindrance for the process to be studied. Few earlier works report on the electrochemical behavior of TiO_2 in aqueous as well as in nonaqueous media but the observations were not conclusive [7–9]. It is important to mention that the mode of synthesis, electrode preparation, electrolyte conductance and the exposed surface could make a significant difference in the electrochemical activity of TiO_2.

In the present work, TiO_2 nanoparticles are doped with C, N and S by adopting independent synthesis methodologies. The successful incorporation of the dopant into the host was confirmed by X-ray photoelectron spectroscopy and the elemental analysis quantified this addition. The diffuse reflectance UV studies were carried out to observe the induced changes in the electronic structure of TiO_2. This leaves us inquisitive regarding the charge transfer properties across the TiO_2/solution interface. Thereby we report a complete study on the synthesis, characterization and redox behavior studies by the cyclic voltammetric (CV) studies on anion-doped TiO_2 nanoparticles. The CV studies identify both pure TiO_2 and anion modified TiO_2 surface states by individualistic redox peaks. A correlation between pH, band bending and cyclic voltammetry responses has been elucidated.

2. Experimental section

2.1. Synthesis procedure

TiO_2 nanoparticles used for N doping were prepared by hydrothermal method at 120 °C for 10 h with $TiCl_4$ as the starting material [10]. The corresponding autogenerated pressure is about 3 kg/cm^2. These TiO_2 nanoparticles are then heated in a furnace at 600 °C with continuous flow of ammonia gas for 3 h. Thereafter it was allowed to cool to room temperature. Light yellow colored $TiO_{2-x}N_x$ was thus obtained. Below 600 °C the percentage of nitrogen incorporated in the host is found to be very negligible. Carbon-doped TiO_2 was prepared by slow addition of tetra *n*-butyl ammonium hydroxide to cooled 0.25 M solution of $TiCl_4$ until pH reached to 5.5. White slurry was aged for 24 h at room temperature followed by filtration, washing and drying. The white colored product was then calcined at 600 °C for 3 h to get a light brown colored $TiO_{2-x}C_x$. Sulphur-doped TiO_2 was prepared as follows: 2.8 g (0.7 M) thiourea was dissolved in 50 ml of ethanol. The 2.48 ml titanium isopropoxide was added very slowly to the solution which gives white color precipitate. The system was then left for stirring for 2 h at room temperature. Ethanol was then allowed to evaporate at room temperature. The white colored product was then calcined at 600 °C for 3 h to get yellow colored product of $TiO_{2-x}S_x$.

2.2. Equipments and measurements

The electrical conductivity (DC) measurements were carried out using a Keithley 236 source measuring unit and impedance (AC) on a HIOKI (3532-50 LCR meter) impedance analyzer. Powder X-ray diffraction (XRD) pattern of the samples were obtained using Siemens D 5000 with Bragg–Brentano geometry using Cu $K\alpha$ radiation ($\lambda = 1.54056$ Å). TEM micrographs were recorded on a JEOL JEM 100 CX electron microscope coupled with selected area electron diffraction facility. Elemental analysis (C, H, N) was done using an elemental analyser (Model Vario El, ELEMENTAR, Germany). X-ray photoelectron spectroscopy (XPS) studies were carried out on a Kratos X-ray photoelectron spectrometer. The X-ray excitation energy was 1253.6 eV (Mg $K\alpha$) and the spectra were recorded at pass energy of 80 eV. UV-DRS spectra were recorded on a Cintra UV-Vis spectrometer in the wavelength range from 200 to 800 nm. The samples for this study were pelletized with KBr taking KBr as the reference. Electrochemical measurements were made on Autolab PGSTAT 30 in a standard three-electrode cell using Ag/AgCl (in aqueous 3 M KCl) as the reference electrode and Pt as a counter electrode. Working electrode was made as circular discs

and the sample holder with the above electrodes was fabricated indigenously. Electrical contacts were established by fixing Pt wires as leads on a Perspex holder by using conductive silver paint. Exposed areas of the back contact and edges were carefully sealed with epoxy resin. The working electrode area was about $0.3\,cm^2$ for each sample. Aqueous electrolytes with 10% ethanol solution were adjusted to pH 2, 6.5 and 10 with H_2SO_4 and KOH, respectively. Ethanol plays the role of a selective scavenger for holes and it is added to avoid $e–h^+$ recombination, whereas electrons are transferred predominantly to dissolved oxygen.

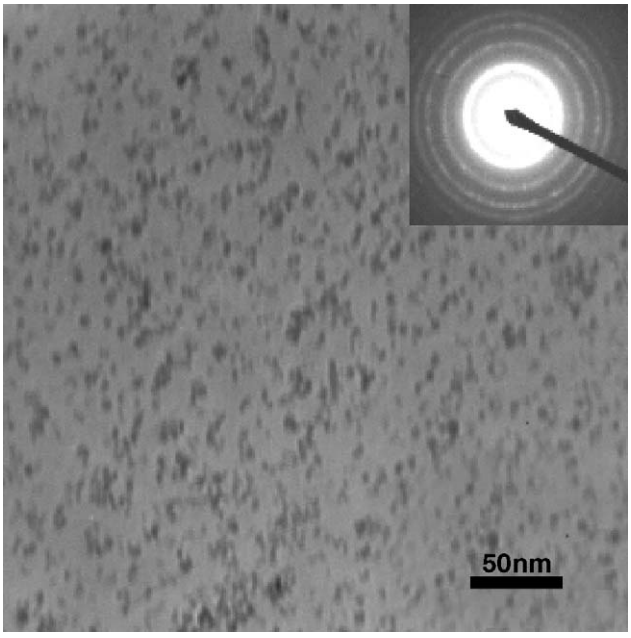

Fig. 1. Transmission electron micrograph of the nano-TiO_2 prepared by hydrothermal method at 120 °C. Inset shows the selected area electron diffraction of the sample.

3. Results and discussion

Fig. 1 shows the transmission electron microscopy (TEM) image of TiO_2 nanoparticles and inset shows the corresponding selected area electron diffraction pattern indexed to anatase (JCPDS Card no. 21-1272). The size of the nanoparticles lies in the range of 3–14 nm.

Fig. 2(a)–(c) represents the TEM image for the N-, S-, C-doped TiO_2 samples. The average particle sizes for all the samples are found to be around 12–15 nm. Table 1 presents the summary of results obtained by characterization of doped and undoped TiO_2 samples. The elemental analysis of the three samples shows the percentage of each of the anionic dopants in TiO_2.

Fig. 3(a)–(c) represents the XRD patterns for the N-, C-, S-doped samples. XRD patterns of undoped and doped TiO_2 did not differ significantly except for a slight variation in the c-axis that suggests a lattice expansion along the c-axis due to the anion incorporation. The crystallite sizes calculated from the Scherrer equation increased for doped samples. This is expected as the doped samples were subjected to heat treatment during the doping process.

Thermo-emf studies on all these samples show that the materials are all n-type with electrons as the majority carriers [11,12]. The DC conductivity for the doped samples increased as compared to the pure oxide. The activation energies E_a were calculated from the $\ln\sigma$ vs. $1/T$ Arrhenius plot obtained from the temperature-dependent conductivity studies. The values show a decrease in the doped samples compared to the pure TiO_2. These observations suggest that doping has increased the electrical conductivity. AC impedance spectroscopy studies were carried out on these materials to give an idea on the type of species responsible for this conductivity behavior.

Fig. 4(a) and (b) shows typical Z'' vs. Z' plot for pure TiO_2 and N-doped TiO_2 samples. It is found that the

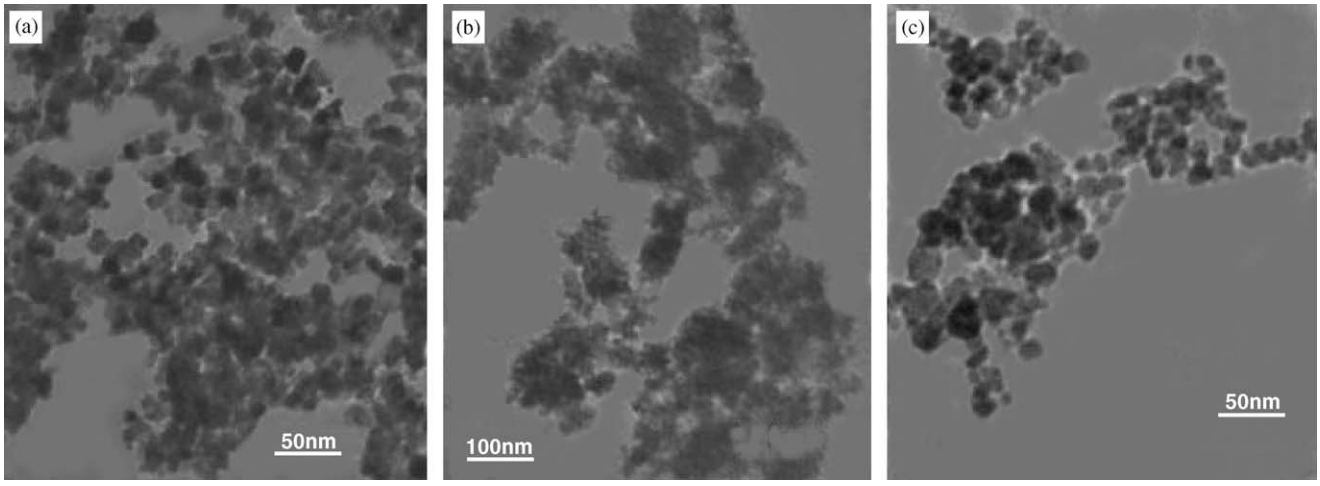

Fig. 2. TEM micrographs of the doped samples: (a) N-doped, (b) S-doped and (c) C-doped TiO_2.

Table 1
Parameters obtained from characterization techniques for $TiO_{2-x}M_x$

Sample	% Incorporated[a]	Lattice parameter[b] (Å)	Crystallite size[c] (Å)	Activation energy[d] (eV)	Band gap[e] (eV)	XPS core level (eV)
TiO_2		$a = 3.779$ $c = 9.488$	82	0.97	3.25	458.80 (Ti2*p*)
TiO_2-N	3.32	$a = 3.776$ $c = 9.508$	96	0.82	3.24 (TiO_2) 2.51	396.32 (N2*p*)
TiO_2-C	3.21	$a = 3.777$ $c = 9.513$	131	0.84	2.85	281.82 (C1*s*)
TiO_2-S	0.46	$a = 3.774$ $c = 9.489$	109	0.87	2.88	164.32 (S2*p*)

[a]Amount of dopants estimated from elemental analysis.
[b]From the *d* values of XRD pattern.
[c]From XRD data using Scherrer formula.
[d]From DC conductivity measurements using Arrhenius plot.
[e]Optical band edge from UV absorption studies.

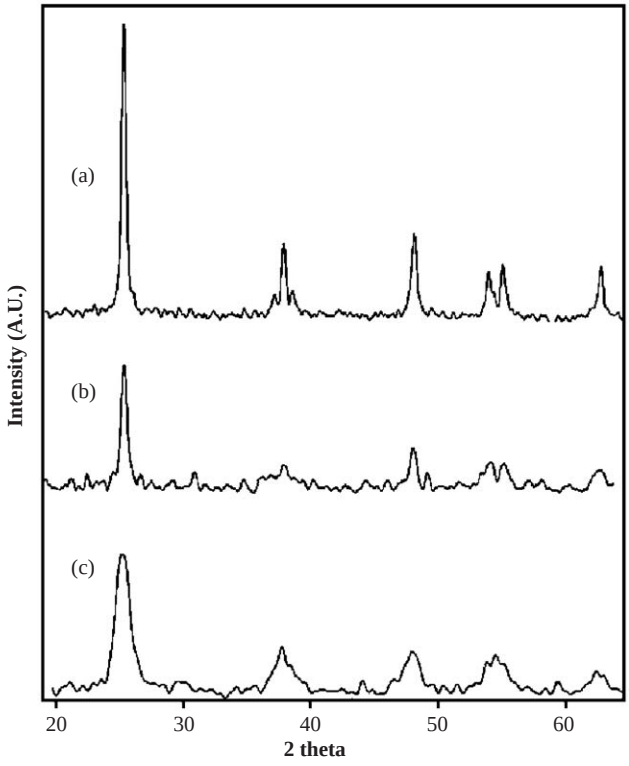

Fig. 3. XRD patterns of the: (a) N-doped, (b) C-doped and (c) S-doped samples.

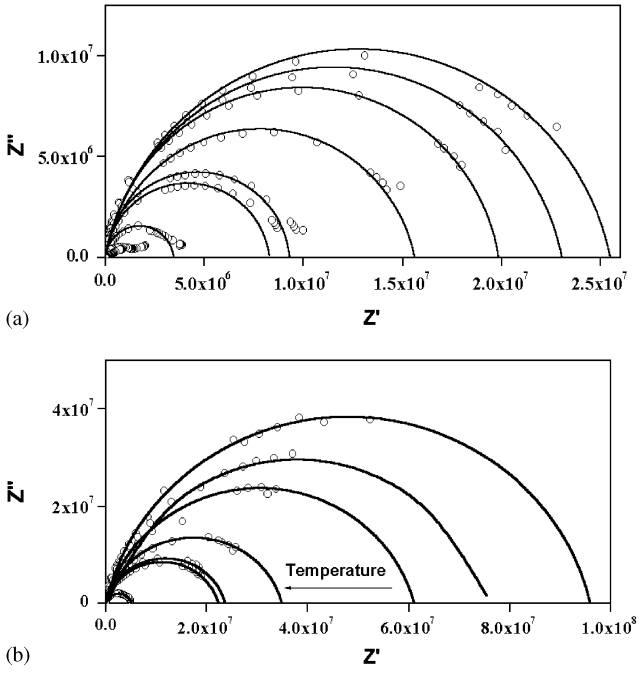

Fig. 4. (a) Cole–Cole plot for TiO_2 impedance spectra measured at different temperatures from RT to 350 °C. (b) Cole–Cole plot for N-doped TiO_2 nanoparticles.

conductivity behavior of the nanosized $TiO_{2-x}N_x$ particles are dominated by grain boundaries. The XPS binding energies of the core level in all the samples indicate the successful incorporation of the dopants into the lattice. As given in Table 1, the binding energy positions of the corresponding core levels in the N-, C-, S-doped TiO_2 and pure TiO_2 indicate the corresponding binding. These are in concurrence with our data obtained from conductivity and absorption studies.

Fig. 5 shows the UV-DRS (UV-visible diffuse reflectance spectroscopy) spectra of undoped and doped TiO_2 samples. A noticeable shift in the absorption edges in the case of doped samples was observed. The optical absorption data was deduced from the Kubelka–Munk function calculated for the TiO_2 and the doped samples from the DRS spectra [13]. Doping of N, S, C anions narrows the band gap of TiO_2 and this feature was more evident in the nitrogen-doped TiO_2 compared to C and S. The notable and significant feature was the N-doped TiO_2 showing two band transitions. The first one was in

the UV region (385 nm), which is accounted for the TiO_2 fundamental band transition and the second in the visible region (495 nm) a resultant of nitrogen doping. This observation from UV-DRS results confirms the presence of two different surface states characteristic of pure TiO_2 and doped TiO_2. In the forthcoming paragraphs, while dealing with electrochemical studies, this distinction between two surface states was reflected as individualistic redox peaks. In contrast, the C- and S-doped samples did not show a sharp absorption edge as observed for pure TiO_2. This would imply that doping introduces electronic states in the band gap that are spread across the band gap, resulting in a diffused absorption spectrum.

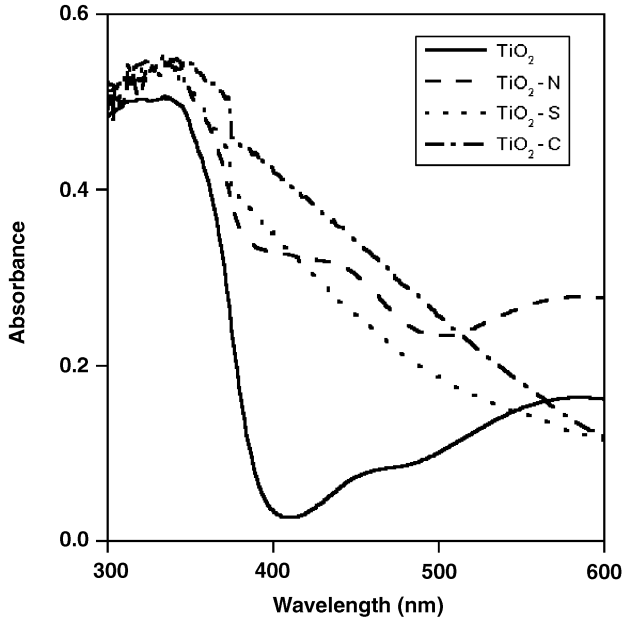

Fig. 5. UV-visible diffuse reflection spectra of undoped and doped TiO_2.

Fig. 6(a) shows the cyclic voltammogram (CV) of pure TiO_2 by a dominant faradic transfer with low capacitance and low faradic resistance [13]. There were no redox peaks at acidic, neutral and alkaline pHs of the experimental solutions. In the forward anodic scan from -1.5 to 2.0 V vs. Ag/AgCl, the current rises steeply with potential but in the reverse scan the cathodic current crosses over at around 0.0 V and forms a loop-like CV response. If the bias voltage shifts the CB from E_{co} (energy level at open-circuit conditions) to E_c (energy level at short-circuit conditions), then the potential scan from -1.5 to 2.0 V ($\Delta V = 3.5$ V; band gap = 3.23 eV), refers to the actual displacement of E_{Fn} (Fermi level) relative to E_c, the bias voltage.

The negative scan could drive the E_{Fn} towards E_v (energy level close to the valence band, i.e., at about 2.0 V) in case of symmetric CV, but this did not happen in the present case. Instead, the E_{Fn} lies close to 0.0 V at which current reversal occurs. If the initial gradient in Fermi level tries to attain equilibrium by driving the electrons to the low energy level, then it appears that the E_{Fn} lies much above the E_v level, followed by hole–charge recombination, which tends to reduce the electron density. This would imply that the energy is pinned at about 0.0 V (band pinning potential) thereby any further continuation of cathodic current would be an energetically unfavorable process, leading to a current reversal.

Fig. 6(b)–(d) show the CVs of doped $TiO_{2-x}M_x$ where $M = C$, S, N; against the poor response of TiO_2 electrode, the doped TiO_2 electrodes show an array of redox peaks indicative of high electrochemical

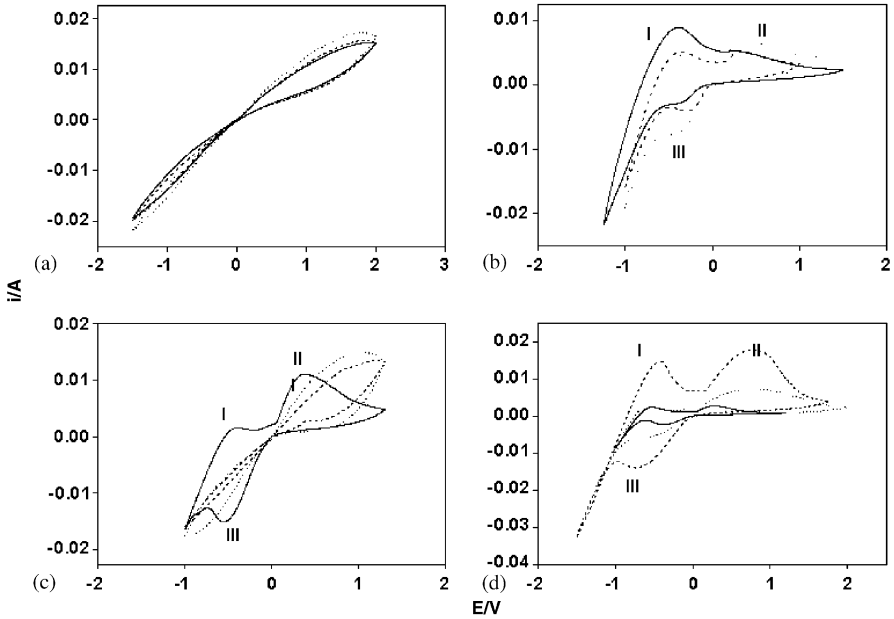

Fig. 6. CVs of: (a) undoped TiO_2; (b) $TiO_{2-x}C_x$; (c) $TiO_{2-x}S_x$; and (d) $TiO_{2-x}N_x$ at various pHs; (——) pH 2, (- - - - -) pH 6.5, and (……) pH 10.

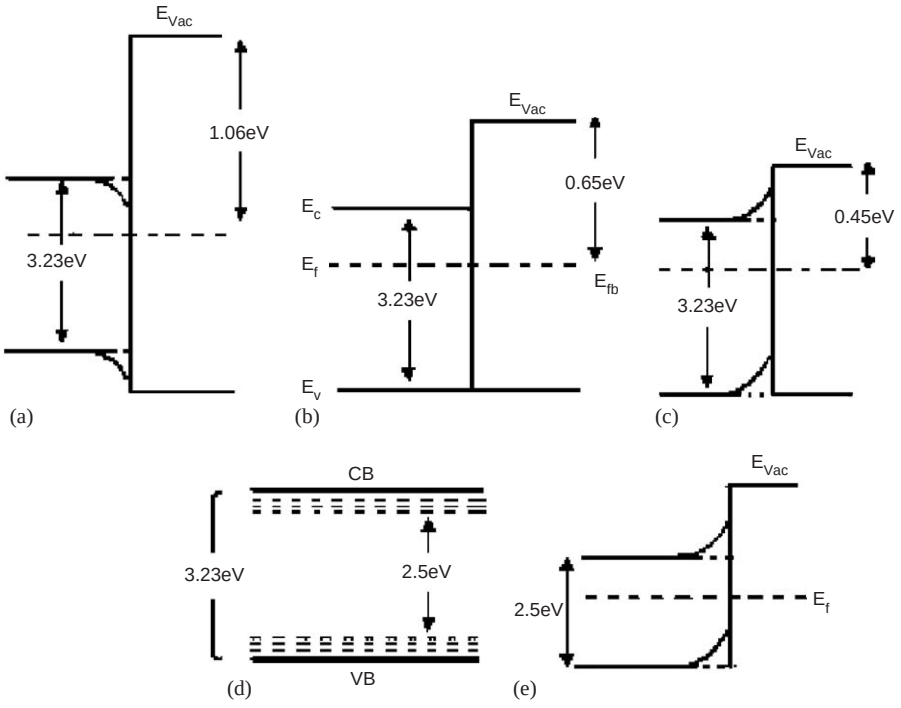

Fig. 7. Hypothetical band pinning diagram at the semiconductor–electrolyte interface when the pH of the solution (a) is 2, where accumulation of charges result, and (b) is 6.5, a flat band situation where E_f is in equilibrium, and (c) is 10, where depletion layer results. (d) The band diagram of the semiconductor after N doping, which introduces intermediate levels, and (e) the corresponding band bending plot of the N-doped TiO_2–electrolyte interface.

Table 2
Peak potentials (in volts) for the three doped samples at different pHs at a scan rate of 50 mV/s (I, II, III denote peaks shown in Fig. 6)

pH	$TiO_{2-x}N_x$			$TiO_{2-x}C_x$			$TiO_{2-x}S_x$		
	I	II	III	I	II	III	I	II	III
2	−0.529	0.277	−0.356	−0.510	0.256	−0.370	−0.392	0.379	0.561
6.5	−0.538	0.478	−0.750	−0.515	0.343	−0.292	—	—	—
10	−0.593	0.754	−0.620	−0.500	0.377	−0.421	—	—	—

reactivity. The lowering of activation energies of doped samples concurs with the CV results. The doping of C, S, and N creates new surface states (E_{FS}) and these surface states result in new energy levels in the band gap providing a favorable pathway for electron transfer between the semiconductor electrode and the acceptor species in solution.

Fig. 7(a)–(e) are typical representations of the reduction in band gap of TiO_2 by doping with nitrogen and the introduction of new surface states or intermediate levels and the corresponding band bending in presence of conducting electrolyte which initiates redox charge transfer reactions. As E_{Fs}, and consequently E_{Fn} progresses closer to E_c, the recombination via the C_b level starts to become significant, and it will be more important than the recombination via surface states (ss), thus reducing the charge transfer resistance and forming the peak characteristics of the pattern.

Table 2 presents the peak potentials of two anodic and a cathodic peak for $TiO_{2-x}M_x$ samples at pHs 2, 6.5 and 10. Peak I in all the CVs (Figs. 6(b)–(d)) corresponds to reduction of Ti^{4+} to Ti^{3+} of $TiO_{2-x}M_x$ and this reduction step was electrochemically irreversible and chemically reversible. It occurs around −0.5 V in $TiO_{2-x}N_x$ and $TiO_{2-x}C_x$ samples. This potential has been identified as the conduction band potential ($V_{cb} = -0.58$ V vs. SCE at pH 3) and in absence of any capacitance, this value represents the electrochemical potential (V) [13]. Peaks II and III correspond to the oxidation and subsequent reduction of dopant species occupying surface states much different from that of pure TiO_2. Peak II occurs at positive potentials in all the samples. This concurs with the earlier report on the photoelectrochemical work where the onset potential was −0.1 V for N-doped and −0.4 V for undoped TiO_2 [6].

The cathodic peak III occurs at negative potentials and the absence of cross over current in these CVs confirm the distribution of energy states between the nitrogen surface states close to VB compared to pure TiO_2 surface states rather than pinning the band energy. For the typical $TiO_{2-x}N_x$ sample, the ΔE_p (potential difference between anodic (II) and cathodic (III) redox couple) increases with increasing pH from $0.633 < 1.228 < 1.374$ V. This trend indicates that the reactions tend to become irreversible with pH. To have effective harvesting of solar light, back reactions are ill advised and unwanted. The electrochemical irreversibility of pure TiO_2 surface states and the quasi-reversibility of doped $TiO_{2-x}N_x$ surface states was a significant result as it provides a pathway for mutual implementation of electrochemistry in terms of semiconductor physics, which in turn is highly beneficial to solar energy conversion.

The effect of pH on peak potentials in the CVs of doped samples was evident by the shift of potentials with pH (Table 2) and likewise, the effect of pH on band bending was presented in Fig. 7 for N-doped TiO_2. At pH 6.5, an equilibrium situation prevails, i.e. the Fermi level of electrons in the substrate equilibrates with the electrochemical potential in the outer circuit and there were no band edge bending in this case. At pH 2, the E_c shifts downward as the adsorption of positive ions tend to shift the band edge positive and in acidic pH, the protons are plenty. The band gap was evaluated to be 1.06 eV and the anodic peak appeared at 0.277 V while corresponding cathodic peak appeared at −0.356 V and the peak currents were comparably less than in other cases. At pH 11, the other extreme case, where hydroxyl ions were abundant, the negative charged ions shift the band edge towards negative direction and the band gap value reduced to 0.45 eV. Here the anodic peak appeared at the most positive potential (0.754 V) while the cathodic peak appeared at the most negative potential (−0.620 V) which indicates that the anodic reaction was energetically favored.

In the case of C-doped sample, the effect of pH on CV response could be understood on the same lines as in N-doped one. The situation was different for S-doped one where there were no redox peaks at pH 6.5 and 10. This could be explained as due to the formation of a passive film on the surface of $TiO_{2-x}S_x$ electrode, which inhibits the charge-transfer process. This observation was validated by the possibility of competitive adsorption of OH^- and SH^- ions on the electrode surface.

4. Conclusions

1. $TiO_{2-x}M_x$ ($M = S, C, N$) nanomaterials were shown to exhibit different optical, electronic and electrochemical properties when compared to undoped TiO_2.
2. Anionic dopants introduce new surface states or polarizations in TiO_2 which provide energetically favorable reaction kinetics inducing charge transfer across the titania/solution interface which otherwise was a polarizable interface.
3. The electrochemical irreversibility of TiO_2 surface states and quasi-reversibility of doped TiO_2 surface states confirm the prevention of back reaction and charge–hole recombination.
4. Based on the absorption studies and CV measurements plausible band diagrams have been proposed to explain the behavior of the doped materials.

Acknowledgment

Authors acknowledge the financial support of CSIR Network Program. KMR, BB and MJ thank CSIR, India for the research fellowships.

References

[1] L.M. Peter, K.G.N. Wijayantha, D.J. Riely, J.P. Waggett, J. Phys. Chem. B 107 (2003) 8378.
[2] (a) Y. Ichihashi, H. Yamashita, M. Anpo, Funct. Mater. 16 (1996) 12;
(b) H. Kisch, L. Zhang, C. Large, W.F. Maier, C. Antonius, D. Meissener, Angew. Chem. Int. Ed. 37 (1998) 3034.
[3] (a) E. Hendry, F. Wang, J. Shan, T.F. Heinz, M. Bonn, Phys. Rev. B 69 (2004) 081101;
(b) Z. Yuan, J. Jia, L. Zhang, Mater. Chem. Phys. 73 (2002) 323.
[4] (a) R. Asahi, T. Morikawa, T. Ohwaki, Y. Taga, Science 293 (2001) 269;
(b) T. Umebayashi, T. Yamaki, H. Itoh, K. Asai, Appl. Phys. Lett. 81 (2002) 454;
(c) A. Sakthivel, H. Kisch, Angew. Chem. Int. Ed. 42 (2003) 4908.
[5] (a) A. Bisquert, M. Zaban, I. Greenshtein, Mora-Sero, J. Am. Chem. Soc. 126 (2004) 13559;
(b) J. Bisquert, V.S. Vikhrenko, J. Phys. Chem. B 108 (2004) 2312;
(c) J. Bisquert, V.S. Vikhrenko, J. Phys. Chem. Chem. Phys. 5 (2003) 5360.
[6] T. Lindgren, J.M. Mwabora, E. Avedano, J. Jonsson, A. Hoel, C.G. Granquist, S.E. Lindquist, J. Phys. Chem. B 107 (2003) 5709.
[7] M. Koelsch, S. Cassaignon, J.F. Guillemoles, J.P. Jolivet, Thin Solid Films 403 (2002) 312.
[8] M. Koelsch, S. Cassaignon, C. Ta Thanh Minh, J.F. Guillemoles, J.P. Jolivet, Thin Solid Films 451 (2004) 86.
[9] X. Gao, H. Zhu, G. Pan, S. Ye, G. Pan, S. Ye, Y. Lan, F. Wu, D.J Song, J. Phys. Chem. B 108 (2004) 2868.
[10] K. Madhusudan Reddy, D. Guin, S.V. Manorama, A. Ramachandra Reddy, J. Mater. Res. 19 (2004) 2567.
[11] F.J. Morin, Phys. Rev. 83 (1951) 1005.
[12] F.J. Morin, Phys. Rev. 93 (1953) 1195.
[13] F. Fabregat-Santiago, I. Mora-Seró, G. Garcia-Belmonte, J. Bisquert, J. Phys. Chem. B 107 (2003) 758.